EXPERIMENTS AND ALGORITHMIC MODEL ANALYSIS OF DRAINAGE EVOLUTION

Dr. N.L. Dongre, IPS, Ph.D., DLitt

Figure.1: The water fall on Dudhi river of Pachmarhis (Pathalkot) India. The generation of drainage in subduction zones, Magmas were consolidated in shape of Columnar Jointing . Magmas were formed by partial melting of the earth's mentle. The melts segregates and moved through the crust to form volcanic intrusions.

Abstract- *To obtain the authenticity of drainage evolution experiments and mathematics- algorithmic model analyses has been executed. While experiments, CO_2 gas was generated by the yeast fermentation of sugar in an elastic layer of gelatine gel confined between two glass plates are observed and analyzed theoretically. The CO_2 gas pressure causes the gel layer to fracture. The gas produced is drained on short length scales by diffusion and on long length scales by flow in a fracture network, which has topological properties that are intermediate between river networks and hierarchical-fracture networks. A simple model for the experimental system with two parameters that characterize the disorder and the intermediate (river-fracture) topology of the network was developed and the results of the model were compared with the experimental results.*

Keyword: - Hierarchical, fluids hydrodynamic, Magmas, hydrocarbons, Hele-Shaw cell, nucleation, chemical equilibrium.

Introduction-The evolution of bandritic, hierarchical rivers drainage networks are the responses of physical systems to the transport of fluids, substances dissolved in fluids or charge. Such directed networks are efficient transport systems and they have characteristic statistical properties [Banavar, J. R., Maritan, A. and Rinaldo, A. 1999]. It has been postulated that river networks and the landscapes associated with them

Figure.2:- The Sonbhadra River (Pachmarhis) India, evolution system. The generation of drainage in Magmas and organic rich Basalt rocks is focus of physical, chemical and Geological details. This generic phenomenon is part of drainage evaluation system, the solid is under confining stress and a fluid is generated internally in the solid and above some length scale, migrated through fractures generated in the solid.

minimize hydrodynamic energy dissipation [Dongre, N.L. 2013]. The evolution of river networks is controlled primarily by erosion, an interaction between flowing water and the landscape that does not extend beyond the local drainage basin. Localized Fracture networks are strain responses to stress beyond the elastic limits of solids and the fracture network characteristics can reveal the nature of the elastic loading, be it external shear, compression or tension, or generated by material shrinkage or by over pressured fluids inside the solid [Sibson, R. H. 1996]. Even if the fluid pressure in fractures is increased only locally, the elastic interactions are *long ranged* and local pressure increases may have long-range effects such as triggering earthquakes [Davies, J. H. 1999, Miller, S. A. 2000]. Horton, investigated for many years, the statistical topology of river networks the statistical description of fractures has only recently been extended to fracture network topologies.

Hydraulic fracturing, used by the petroleum industry to enhance the permeability of reservoir rocks, is induced by injecting a fluid at high pressure into the rock via a cased, cemented and perforated well. In some geological processes large fluid pressures are generated pervasively inside very large rock volumes and the fluid is expelled and transported out of the system. For example, in subduction zones hydrous minerals are subject to increasing pressure and temperature until they are no longer thermodynamically stable and form anhydrous minerals and hydrous fluids with a smaller solid volume but larger total (solid plus fluid) volume [Davies, J. H. 1999]. Magmas are formed by partial melting of the Earth's mantle, the melt segregates and moves through the crust to form volcanic intrusions, (Fig: 1). As they are progressively burried, organic rich shales are heated and the organic material is thermally decomposed into low-molecular-mass hydrocarbons with lower densities and viscosities. The transport of these lighter hydrocarbons through the virtually impermeable shale to adjacent high-permeability rock

layers is called primary migration and if the shale layer is thick the hydrocarbon drainage must occur via fractures generated in the shale.

Even though the generation and drainage of fluids in zones of subduction, magmas and organic rich shales have each been extensively investigated, the concentration of these investigations has been on physical, chemical and geological findings rather than generic phenomena. In all of these systems, the solid is under confining stress, a fluid is generated internally in the solid and above some length scale, the fluid migrates through fractures generated in the solid(Fig:2). Here, a set of experiments, a simple theory and an algorithmic model for a system with these characteristics are presented. This system demonstrates the evolution of a new class of networks, drainage fracture networks that are intermediate between river networks and hierarchical-fracture networks. A river drainage network with loops has been mentioned as topologically possible, but less efficient, network in studies of transport efficiency [Banavar, J. R., Maritan, A. and Rinaldo, A. 1999]. Here it is explored that the physical reasons why they exist in experiments and possibly in Nature.

Experimental set-up.-The experiment consists of a Hele-Shaw cell with a gel containing water, gelatin, sugar and yeast. When the yeast consumes the sugar it produces CO_2 and CO_2 bubbles nucleate and evolve into gas-filled fractures. The gas is transported with these cracks to the edges of the gel layer. The Hele-Shaw cell consists of two $300 \times 300 \times 10$ mm glass plates clamped together and separated by 3 mm.

The Hele-Shaw cell was filled with liquid gelatine solution after cleaning the inner surfaces with detergent and distilled water to ensure good adhesion between gelatine and glass. A gelatin solution was prepared by dissolving 58 g of gelatine sheets (from Gelita) in 1 dm^3 of boiling water (100°C). 7.5g of sugar was dissolved in the gelatine solution, which was then cooled to 30 °C, mixed with 2.5 g of baking yeast and stirred well to homogenize it. Half of the liquid solution was poured into an area of $L \times L$,$L = 250$ mm of the Hele-Shaw cell and the other half was poured into a bottle connected to a gas volume meter. Both solutions were kept in a refrigerator at 6 °C for 10 hours to obtain a solid, homogeneous gel. It is assumed that the yeast particles are homogeneously distributed on large scales and variations in the particle size and local number density (and gas production rate) are treated as quenched disorder.

Four experiments under same conditions were conducted at room temperature (17 ± 1 °C), where the gelatine is a transparent, brittle, nearly elastic solid [Di Giuseppe, E., Funiciello, F., Corbi, F., Ranalli, G. and Mojoli, G. 2009]. Two experiments (Exp_1,Exp_2) were performed with the same concentration of yeast and sugar (as described above). In the other two experiments (Exp_3,Exp_4) half and double the amounts of yeast and sugar were used. At 17 °C, yeast is activated, consumes sugar and produces CO_2 gas.

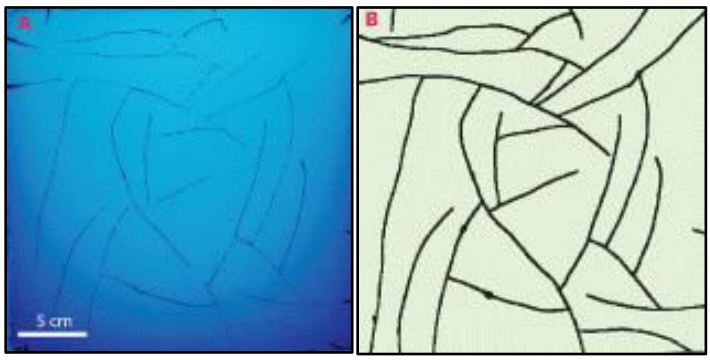

Figure. 3: During the processed experiment, actual optical images of Exp_1. A: actual image of fracture pattern at time t = 22 h. B: processed binary image used for extended analysis of network topology and geometry. The boundary of the gelatine layer is not limited and it is under the drainage perimeter. (After- Kobchenko. Maya, *etl* 2013)

Fracture nucleation and propagation was imaged every minute at a resolution of 9 pixels/mm. Measurements of the bubble sizes and fracture apertures have an estimated accuracy of ±0.1 mm. Digital image correlation analysis showed that the motion of the camera was $\leqslant 1$ pixel length.

Results.-After ≈2 hours fracture nucleation and growth began and the fractures transported gas to the edges of the gel. Development of the fracture pattern continued for an additional 20 hours until the "final" pattern, shown in fig.3 was obtained.

In parallel with the fracture experiment, the bottle for measuring the gas production rate, γ, was held at the same temperature as the Hele-Shaw cell. In the Exp_1 and Exp_2 the gas production rate increased steadily from zero, after ≈2 h the production rate had reached ≈0.7 ml/h and at 20 h it peaked at ≈2 ml/h.

***Dynamics of fracture nucleation and growth*:** The initial tiny bubble comes out in the gel after approximately 2 hours from the starting of the experiment and 10–20 bubbles nucleated in the next 20 hours. Bubbles grew till they reached a diameter of near about $l_0 = 2.3 \pm 0.2$ mm and then converted into stretched cracks with sharp tips after 12 ± 3 min. But, for about 50% of the fractures, starting bubble nucleation and growth stage was not found with the image resolution in these experiment. Crack tips propagated with increasing velocity, at both ends of the fractures, unless they became blunted or closely approached the boundary of the gelatine layer or another crack. During the free propagation regime, before cracks started interacting with other cracks or with the boundary, the crack length evolved with time as

$$l = l_0 \exp(t/\tau), \tag{1}$$

where t is the time since fracture nucleation. The increase in the timescale, τ with increasing gas generation rate, γ, could be represented by $\tau = 0.54/\gamma - 0.20 \pm 0.017$ h. Each crack tip either propagated until it connected to another fracture or reached the gel boundary, or it slowed down and ultimately stoped inside the gel matrix, creating a dead end. When a fracture was not connected to other fractures or the gel boundary, its aperture a increased with time due to increasing gas pressure until a maximum aperture of approximately 3 mm was reached along most of the fracture length. When two cracks intersected their apertures changed rapidly indicating pressure equilibration. When a crack reached the gel boundary, its aperture collapsed as the gas drained from the system in less than one second. Once a crack formed, it continued to serve as an intermittent drainage pathway that closed and opened. New fractures nucleated and propagated until a steady-state fracture pattern stabilized, see Fig. 3A.

The development of the fracture pattern was analyzed, the fractured gelatine images were processed such that all pixels that were once covered by a fracture were preserved in accumulated images that denotes the development of the fracture network. The final accumulated fracture pattern for experiment Exp_1 is displayed in Fig. 3B.

In most cases, both crack tips propagated linearly, with about the same velocity, until they reached a distance of $\lambda_e = 10 \pm 5$ mm from another crack or a distance of 20 ± 5 mm from the gel edge. In such instances they would slow down, speed up, or change direction, depending on the circumstances. It will refer to λ_e as the elastic interaction length.

The movement of tracer particles in the gel and of the gel edges was tracked using digital image correlation. While opening the cracks, new volume is generated in the system, but no calculated expansion of the gel in the plane of the Hele-Shaw cell was observed. However, by using an LVDT displacement sensor, It was found that the glass plates confining the gel moved in the direction perpendicular to the plane of the Hele-Shaw cell plane, allowing the gel to increase in thickness. The total deflection of the plates corresponded to a total volume increase of $(1.9 \pm 0.1) \times 10^{-6}$ m^3. Since the gel is essentially incompressible, this corresponds to the volume of the gas trapped in the fractures and the largest total volume of the open fractures was estimated from image analysis to be $(2.2 \pm 0.1) \times 10^{-6}$ m^3.

***Spatial distribution of fracture nucleation*:** To analize the mechanisms of crack formation and growth, it was analyzed to what extent new fractures nucleate either in the middle of unfractured domains, near existing fractures, or randomly. When a crack formed it was assigned a number indicating the order in which it was formed as shown for experiments Exp_1 and Exp_2 in Fig. 4A and B. Distance maps as shown in Fig. 5 were computed where the colour indicates the distance $r(x,y)$ from the coordinate (x,y) to the closest fracture or free boundary. For each nucleation event i, the distance r_i, position, (x_i,y_i) and gradient $\nabla r(x_i,y_i)$ were determined just before nucleation occurred. On a line through (x_i,y_i) in the direction $\nabla r(x_i,y_i)$, the local maximum of r is denoted $r_{max,i}$.

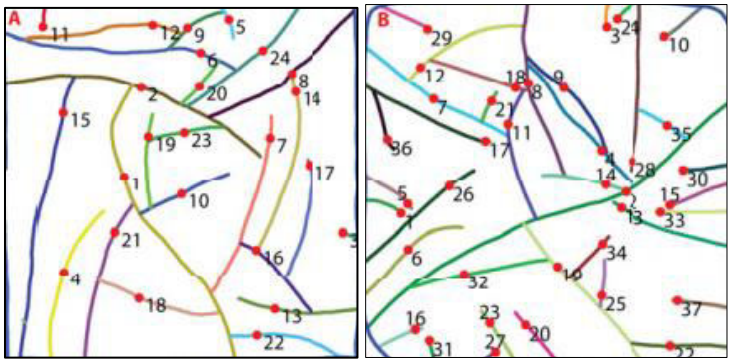

Figure. 4: A, B: nucleation sites and fracture indicating in Exp_1 (A) and Exp_2 (B). The fractures are differed by their colours and their numbers shows the order in which they presented. The red circles mark the nucleation sites. (After- Kobchenko. Maya, *etl* 2013)

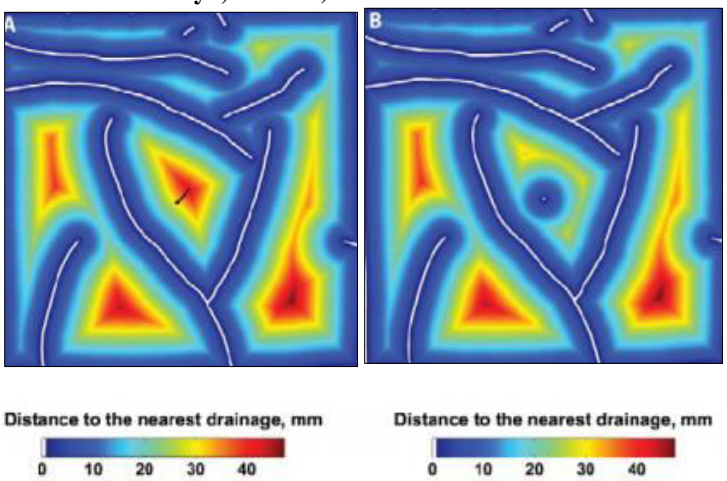

Figure. 5: The diagram of distance, $r(x,y)$ to the adjacent fracture right pre and post of the nucleation of fracture 10 in fig. 4_A. A: a line from (x_{10},y_{10}) in the direction $\nabla r(x_{10},y_{10})$ up to the position of the local maximum of r, $r_{max,10}$ is marked in black. Panel B exhibits how the distance diagram is altered immediately following the nucleation of fracture 10. (After- Kobchenko. Maya, *etl* 2013)

The normalized distance $r_i/r_{max,i} = 0$ or 1 correspond to nucleation at an existing fracture or in the middle of an un fractured domain. The cumulative distribution $N(r/r_{max} > r_i/r_{max,i})$, which is plotted in Fig. 4, characterizes the degree of randomness in the locations of the nucleation sites and is fitted by $N = (r_i/r_{max,i})^{\mu}$, $\mu = 1.94$. $\mu \leq 1$ (the exact value depends on the shape of the un fractured area) corresponds to completely random nucleation and $\mu \to \infty$ corresponds to deterministic nucleation in the middle of an un fractured domain. The inset shows the cumulative distribution of r_i and demonstrates that there is a minimum distance between nucleation sites and pre-existing fractures.

***Fracture growth direction*:** The direction of fracture propagation from the nucleation point was measured and found that the distribution of angles between the fracture directions and the distance gradients, $\nabla r(x_i,y_i)$, was uniform between 0 and 90 degrees.

***Analysis of steady-state fracture pattern*:** The steady-state fracture network shown in Fig. 3B was skeletonized and all intersections of fractures (blue circles in Fig. 7A) and fracture tips (red squares in Fig. 7A) were identified and labeled as *nodes*. A fracture may be divided into *segments* consisting of the part of the fracture between two adjacent nodes or between a node and an end of the fracture and these segments are identified by different colours in Fig. 7A, (the outer boundary is considered to be one continuous segment).

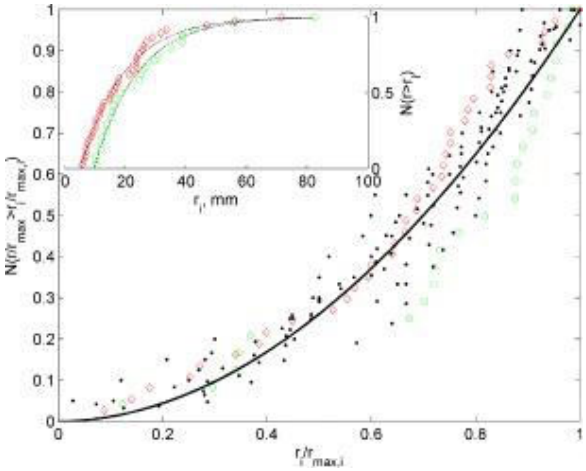

Figure. 6: Cumulative distribution of the normalized distances, $r_i/r_{max,i}$, from nucleation sites to the nearest drainage interface. Green data points correspond to Exp_1, red to Exp_2. The black dots correspond to randomly generated networks using the fragmentation fracture model. The continuous line is a fit of the data using the function $y = x^{\mu}$,μ = 1.94. The inset shows the cumulative distributions of r_i. This indicates that there is a minimum distance between nucleation points and pre-existing fractures, r_{min} of about 5 and 10 mm in the 2 experiments. (After- Kobchenko. Maya, *etl* 2013)

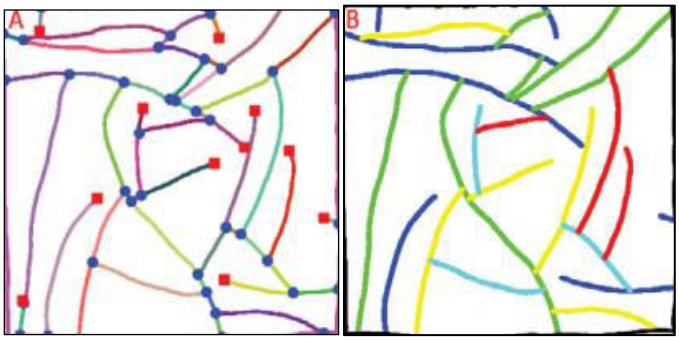

Figure. 7: The fracture network characteristics of Exp_1. A: fracture segments marked with various colours. Blue discs denote junctions between segments and red squares shows dead ends. B: fracture network coloured as per the fracture generation number, n_C, of fracture *C* intersecting fractures *A* and *B*: n_C = max (n_A,n_B) + 1. Black: 0; blue: 1; green: 2; yellow: 3; light blue: 4; red: 5. (After- Kobchenko. Maya, *etl* 2013)

It is measured at each node of the angles between intersecting segments. There were two different peaks: one in the range 180 ± 5° and another in the range 90 ± 10°. By joining segments that intersect at angles about 180°, It is reconstructed that the continuous fractures which formed by propagation from a single nucleation point. This fracture pattern has a temporal order of nucleation (see numbering in Fig. 4). In addition a hierarchical order can be defined such that if fracture C ends at fractures A and B its

generation number is $n_C = \max(n_A,n_B) + 1$, where n_A and n_B are the generation numbers of fractures A and B . The draining perimeter is considered to be generation 0. In the experiments, up to five fracture generations ($n = 5$) were measured. In Fig. 7 B, the fractures of Exp_1 have been colour coded to indicate their fracture generation numbers. A fracture is "younger" than the youngest fracture it forms a junction with. One possible alternative generation numbering scheme emphasizing the drainage aspect of the network would be $n'_C = \min(n'_A,n'_B) + 1$, which corresponds to numbering of river segments in a drainage basin. Using this scheme the highest drainage generation is $n' = 3$.

Discussion and conclusion.-The experimental results were used to propose a mechanism of fracture nucleation and propagation. Thus now demonstrate that the fracture network has intermediate statistical properties between those of river-like and hierarchical-fracture–like patterns.

***A diffusion-nucleation model for fracturing*:** The production of CO_2 provides the energy required for fracturing the gel and the fracture network evolution depends on the coupling between CO_2 transport and elastic interactions in the matrix. The observation that fractures initiate as bubbles far away from existing boundaries suggest that crack nucleation is not determined by elastic interactions. Therefore propose the following diffusion-nucleation model:

1. Most of the generated CO_2 is dissolved into the gel, which consists of 95% water. The solubility and diffusion coefficient of CO_2 in the gel are approximately the same as in pure water, $c_0 = 1.8$ g/l and $D = 1.85 \cdot 10^{-9}$ m^2 s^{-1} . The dissolved CO_2 has negligible mechanical effects on the gel matrix.
2. Bubbles nucleate when CO_2 generation leads to local super saturation in the gel. Nucleation is heterogeneous and only a small super saturation is required.
3. After growing, the bubbles begin interacting elastically with the gel matrix and a transition from bubbles to fractures happens.
4. The resulted fracture propagation is driven by the gas pressure on the fracture walls which induce elastic stresses in the material.

***Growth of a single fracture*:** When a fracture has nucleated, it propagates when the gas pressure exceeds some critical value p_c. When fractures propagate slowly the gas pressure is constant and equal to p_c. Using the ideal gas approximation $pc. = \frac{n_{Co_2RT}}{V} = \text{const}$, the change in fracture volume is

$$\frac{\mathrm{d}V}{\mathrm{d}t} = \frac{RT}{p_c}\frac{dnCO_2}{\mathrm{d}t} \tag{2}$$

The fracture aperture is limited to $a = 3$ mm due to adhesion of the gel to the walls of the Hele-Shaw cell and the volume of gas in the fracture is $V \approx lah$, where l is the fracture length and $h = 3$ mm is the distance between the glass plates. During propagation of a single fracture we assume a constant CO_2 flux, ϕ, over the fracture surfaces

$$\phi = \frac{\mathrm{d}nCO_2}{\mathrm{d}t}\frac{1}{2lth} = \text{const.} \tag{3}$$

The expression

$$l = l_0 \exp\left(\frac{2\phi RTt}{p_c a}\right), \tag{4}$$

for the fracture length can be derived by combining eqs. (2) and (3) and integrating. Here, l_0 is the integration constant, which characterizes the critical length above which a gas bubble evolves into a fracture. This corresponds to eq. (1), which was used to fit the experimental data and comparison of eqs. (1) and (4) indicate that $1/\tau \propto \phi \propto \gamma$.

***Size of unfractured domains*:** Various factors control the final configuration of the fracture network. Since the gas production rate is virtually constant for a long period after the last fracture has

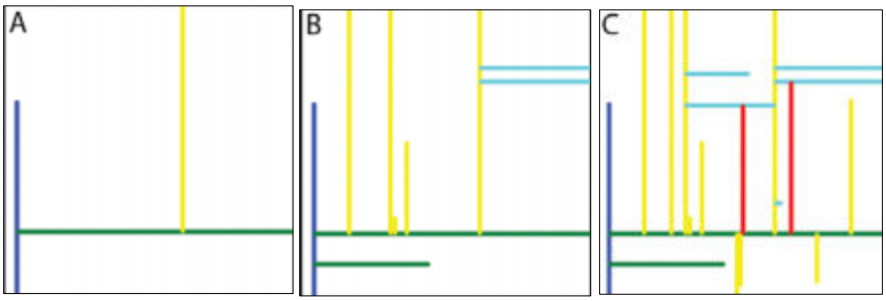

Figure.8 Fragmentation fracture model with $\omega = 0.36$ shown at three stages of evolution, $l_t/L = 2.2,5.1,8.56$. The lines are coloured according to the fracture generation number, n_C, of fracture *C* intersecting fractures *A* and *B*: $n_C = \max(n_A,n_B) + 1$. Black: 0; blue: 1; green: 2; yellow: 3; light blue: 4; red: 5. (After-Kobchenko. Maya, *etl* 2013)

stopped propagating it is assumed that the system reaches a quasi-steady state in which the fracture network drains the gel matrix sufficiently to hinder further fracturing. Using a diffusion-nucleation model, the characteristic size of unfractured domains, for which loss of CO_2 by diffusion is sufficient to prevent nucleation of new fractures can be estimated.

Consider a gel segment bounded by two parallel fractures separated by a distance 2δ. Assuming a constant CO_2 production rate,γ, the steady-state equation for the concentration field in the gel is

$$D\nabla^2 c + \gamma = 0. \qquad (5)$$

Figure.9: Nagduari rift at Pachmarhis (India). Fracture orientation on actual location, horizontal and vertical distance in both directions until it reaches and form a junction with another fracture of the system boundary

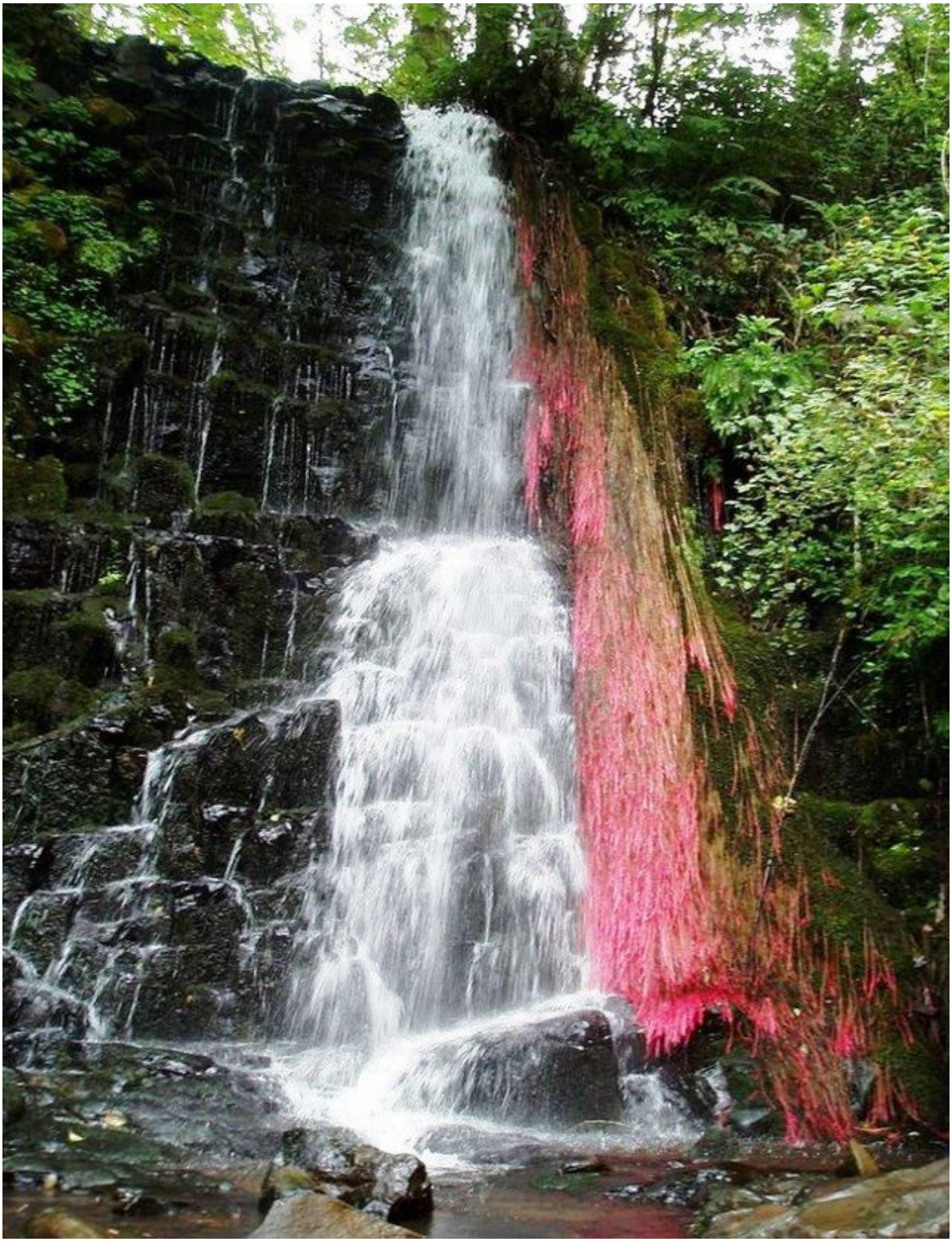

Figure.10: Fall on Denwa River, India. The fracture occurred and increased because it is drained by the joining fracture $(1-\omega)$, it may continue to grow until the other end meets an existing fracture $\omega = 1$ corresponds to all fractures connected at both ends which is typical of a hierarchical fracture pattern.

It is assumed that the flux ϕ of CO_2 across a fracture surface is proportional to the difference between the concentration c of dissolved CO_2 at the surface and the concentration required for chemical equilibrium with the gas pressure $p = k_H c$ in the fracture,*i.e.*,

$$\phi = D\frac{\mathrm{d}c}{\mathrm{d}x}\bigg|x = \pm\delta = k\left(\frac{\mathrm{p}}{\mathrm{k_H}} - \mathrm{c}(\pm\delta)\right), \qquad (6)$$

where k_H is the Henry's coefficient and k is a rate constant of CO_2 evaporation from the gel. The solution of (5) is

$$c(x) = \frac{\mathrm{p}}{\mathrm{k_H}} + \frac{\gamma^{\delta}}{\mathrm{k}} + \frac{\gamma}{2\mathrm{D}}(\delta^2 - x^2). \qquad (7)$$

It is believed that to nucleate a bubble a critical super saturation $c_c = p_c/k_H$ is required. Inserting $c(x = 0) = c_c$ into eq. (7) It can be solved for the critical distance δ_c and find two scaling regimes:

-diffusion limited $(k \to \infty), \delta_c = \sqrt{\frac{2D}{\gamma}\frac{p_c - p}{k_H}} \propto \gamma^{-1/2,}$

-evaporation limited $(D \to \infty), \delta_c = \frac{k}{\gamma}\frac{p_c - p}{k_H} \propto \gamma^{-1}$

It follows that in the diffusion-limited case $\gamma^{1/2}\delta_c$ should have a constant value and $\gamma\delta_c$ should have a constant value for the reaction-limited (evaporation-limited) case. In Exp_1 the mean production rate was γ = 1.6 ml/h and $2\delta_c$ = 22.2 mm ($\gamma\delta$ = 17.76,$\gamma^{1/2}\delta$ = 14.0) and in Exp_4 the mean production rate was γ = 6.2 ml/h and $2\delta_c$ = 10.7 mm ($\gamma\delta$ = 33.2, $\gamma^{1/2}$,δ = 13.3). This is consistent with the diffusion-limited model, but not with the reaction-limited model. The shape of the cumulative distribution function (for $r_i/r_{max,i}$) shown in fig. 6, with μ = 1.94, is also consistent with the diffusion-limited scenario, but not with the reaction-limited model since in the reaction-limited limit $\mu \leqslant 1$.

***Elastic interactions, directed networks and loops*:** The short range of the elastic interactions is a result of the adhesion between the gel and the rigid walls of the Hele-Shaw cell. A three-dimensional solid full of gas-filled fractures will also have a limited elastic interaction length due to the "screening" by open fractures. The elastic interaction between fractures in the model system results in the opening and closing of fracture apertures at junctions, which act as valves to the gas flow. This dynamic process, causing intermittent gas release, will be described in detail in a future communication. The adhesion between the gel and the glass walls of the Hele-Shaw cell also imposes an effective confinement on the system similar to the effects of compressive elastic stress on a three-dimensional system. Under such confining conditions, neighbouring fractures in analogous three-dimension systems will interact in a similar manner —when the aperture of one fracture increases due to increased fluid pressure it will increase the compressive stress on neighbouring fractures and this will reduce their apertures.

It should be noted that although $\delta_c \sim r_{min} \sim \lambda_e \sim 10$ mm in experiments Exp_1 and Exp_2, the similarity between λ_e and the other lengths is fortuitous. The elastic interaction length λ_e does not depend on the gas production rate as do δ_c and r_{min} and elasticity does not control δ_c and r_{min}.

The flow direction of gas follows the direction of the pressure gradient, but due to confinement induces elastic interactions between fractures and adjacent fractures and junctions, which acts as valves when the gas pressure is reduced, the direction of the pressure gradient is not static. Because of the "valve closing" effect, fractures that are connected at one end to a fracture network that reaches the edge of the gel may propagate at the other end until that end also contacts a pre-existing fracture. The end result is a network with loops. A hierarchical-fracture network is ideally fully connected.

***Model of fracture propagation*:** A simple model that captures some of the essential features of our experimental system and incorporates river-like and hierarchical-fracture–like networks as limiting cases was developed (see Fig. 8). A lattice model of size $L \times L$ was used, where L is the size of the gelatine layer. Fractures nucleate and propagate sequentially and form a "final" pattern when the system is completely drained, *i.e.*, when the cumulative fracture length in the pattern exceeds or equals the cumulative fracture length l_t. l_t/L is 8.5 in Exp_1 and 8.7 in Exp_2. The nucleation sites are chosen according to a probability distribution $P(x,y)$ that depends on the distance from the site to the nearest fracture or boundary. We chose a power law distribution such that the probability of nucleating a fracture at site (x,y) is

$$P(x,y) = r(x,y)^{\mu-1} / \sum_{x,y} r(x,y)^{\mu-1} \qquad (8)$$

where $r(x,y)$ is the distance from the nearest fracture or the boundary. This choice is substantiated by the experimental distribution (Fig. 6), where the power law exponent was decided to be $\mu = 1.94 \pm 0.06$. The black dots in Fig.6 show the resulting cumulative distribution of $r_i/r_{max,i}$ of nucleation points for 20 realizations of the model. This demonstrates that although the model was constructed with a different metric from that used to measure μ an exponent of $\mu = 1.94$ makes the model nucleation distribution lie within the range of uncertainty of the experimental nucleation distribution.

When a nucleation site is selected, the fracture orientation is randomly selected as horizontal or vertical. The fracture propagates by the same distance in both directions until it reaches and forms a junction with another fracture or the system boundary (Fig: 9). At this instance the fracture may either cease to grow because it is drained by the joining fracture (with probability $1 - \omega$), or it may continue to grow until the other end meets an existing fracture (with probability ω). $\omega = 1$ corresponds to all fractures connected at both ends which is typical of a hierarchical-fracture pattern (Fig: 10). $\omega = 0$ corresponds to all fractures connected at one end only which is typical of river networks. The probability ω of a network can be deduced from the ratio between the number of dead ends, n_d, and the number of junctions, n_j: $\frac{n_d}{n_j} = \frac{1-\omega}{1+\omega}$ and ω are 0.41 and 0.32 for Exp_1 and Exp_2.

***Conclusion*:** The production and exsolution of CO_2 in a gel-filled Hele-Shaw cell generated a new type of drainage fracture network with topological properties intermediate between those of directed river networks and hierarchical-fracture networks. The valve-like opening and closing of fracture apertures at fracture junctions plays an important role in the formation of this type of fracture network. Diffusion of CO_2 in the gel inhibits the nucleation of new fractures in the vicinity of pre-existing fractures and a simple random nucleation model that takes this and the probability that fracture propagation stops before both ends of the growing fracture reach other fractures, reproduces key characteristics of the experimental fracture network.

References

- Banavar, J. R., Maritan, A. and Rinaldo, A. 1999; Nature 399 130
- Dongre, N.L.,2013; Rationality to the behaviour of river systems and disipation of drainage generated energy, Google Publication.
- Di Giuseppe, E., Funiciello, F., Corbi, F., Ranalli, G. and Mojoli, G. 2009 ; Tectonophysics 473 391
- Davies, J. H. 1999; Nature 398 142
- Horton, R. E. 1945; Geol. Soc. Am. Bull. 56 275
- Hild, F. and Roux, S. 2006; Strain 42 69
- Kobchenko. Maya, Hafver. Andreas, Jettestuen. Espen, Galland. Olivier, Renard. François, Meakin. Paul, Jamtveit. Bjørn, and Dysthe. Dag K., 2013; Drainage fracture networks in elastic solids with internal fluid generation . A Letters Journal Exploring The Frontiers of Physics
- Li, H. L., Wilhelmsen, O., Lv, Y. X., Wang, W. L. and Yan, J. Y. 2011; Int. J. Greenhouse Gas Control 5 1119
- Miller, S. A. 2002; J. Geophys. Res.: Solid Earth 107.
- Sibson, R. H. 1996; J. Struct. Geol. 18 1031.